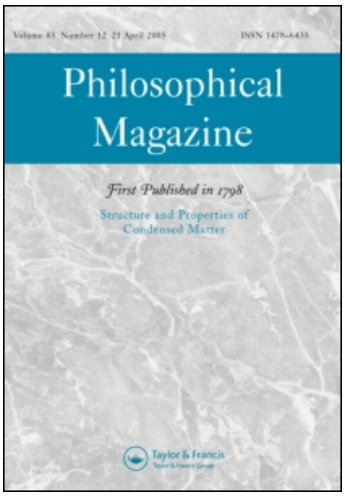

Philosophical Magazine
Publication details, including instructions for authors and subscription information:
http://www.informaworld.com/smpp/title~content=t713695589

Cyclic deformation and fatigue cracking behaviour of polycrystalline Cu, Cu-10 wt% Zn and Cu-32 wt% Zn

P. Zhang [a]; Q. Q. Duan [a]; S. X. Li [a]; Z. F. Zhang [a]
[a] Shenyang National Laboratory for Materials Science, Institute of Metal Research, Chinese Academy of Sciences, Shenyang 110016, China

Online Publication Date: 01 June 2008

To cite this Article Zhang, P., Duan, Q. Q., Li, S. X. and Zhang, Z. F.(2008)'Cyclic deformation and fatigue cracking behaviour of polycrystalline Cu, Cu-10 wt% Zn and Cu-32 wt% Zn',Philosophical Magazine,88:16,2487 — 2503
To link to this Article: DOI: 10.1080/14786430802375634
URL: http://dx.doi.org/10.1080/14786430802375634

Philosophical Magazine
Vol. 88, No. 16, 1 June 2008, 2487–2503

Taylor & Francis
Taylor & Francis Group

Cyclic deformation and fatigue cracking behaviour of polycrystalline Cu, Cu–10 wt% Zn and Cu–32 wt% Zn

P. Zhang, Q.Q. Duan, S.X. Li and Z.F. Zhang*

Shenyang National Laboratory for Materials Science, Institute of Metal Research, Chinese Academy of Sciences, Shenyang 110016, China

(*Received 16 April 2008; final version received 26 July 2008*)

The cyclic deformation behaviour of polycrystalline Cu, Cu–10 wt% Zn and Cu–32 wt% Zn was systematically investigated in the plastic strain amplitude range of 1×10^{-4}–4×10^{-3}. The differences in the cyclic stress–strain (CSS) responses and fatigue cracking behaviour between Cu, Cu–10 wt% Zn and Cu–32 wt% Zn were compared. It was found that the occurrence of a cyclic saturation for Cu–10 wt% Zn and Cu–32 wt% Zn strongly depends on the applied strain amplitude, whereas polycrystalline Cu always displays cyclic saturation. Surface deformation morphologies were analyzed by scanning electron microscopy (SEM). One of the major features observed is that the slip bands become increasingly homogenous with Zn addition. The fatigue cracks were found to frequently nucleate along the annealing twin boundaries (TBs) in Cu–10 wt% Zn and Cu–32 wt% Zn, but not in polycrystalline Cu. Based on these experimental results, the cyclic deformation response and fatigue cracking behaviour are discussed, and a developed TB cracking mechanism is proposed to explain the difference in fatigue cracking mechanisms in Cu, Cu–10 wt% Zn and Cu–32 wt% Zn.

Keywords: polycrystalline copper; Cu-Zn alloys; cyclic deformation; slip bands; grain boundary; twin boundary; fatigue cracking

1. Introduction

During the second half of the last century, especially in the period from the 1960s to the late 1980s, a large amount of research was carried out to investigate the cyclic deformation response of crystalline materials. These studies usually focused on issues on cyclic plasticity [1], fatigue crack nucleation and propagation [2], and the corresponding evolution of dislocation structures during cyclic deformation [3–5]. In addition, these studies covered many different kinds of materials, from single crystals to polycrystals, and from pure metals to alloy systems [6–9].

In the early studies, much attention focussed on the fatigue mechanism of wavy-slip materials, mainly copper single crystals [1,10]. All these investigations revealed that almost all the plastic strain is carried by persistent slip bands (PSBs), which consist of thin lamellae extending in the bulk through the specimens [11]. This feature of cyclic deformation was well explained by Winter [12] and Finney and Laird [7] in terms of

*Corresponding author. Email: zhfzhang@imr.ac.cn

ISSN 1478–6435 print/ISSN 1478–6443 online

DOI: 10.1080/14786430802375634
http://www.informaworld.com

a two-phase model (PSB and matrix). Based on this model, Mughrabi [1] plotted the famous cyclic stress strain curve (CSSC) for copper single crystals with single-slip orientation, and a clear plateau with a resolved saturation shear stress of ~28 MPa was found. Fatigue cracking often initiated along the intrusions or extrusions induced by PSBs in copper single crystals [13,14]. In addition, investigations on polycrystalline copper were widely reported and the existence of PSBs in the interior grains of samples was proved [4]. The fatigue damage mechanisms of polycrystals are, however, relatively complex in comparison with those of single crystals because grain boundaries (GBs) act as obstacles against slip deformation and often become the preferential site for fatigue crack initiation during cyclic deformation [2,15]. Copper bicrystals were employed to clarify the GB effect on fatigue damage by Gopalan and Margolin [16], Hu et al. [17], Hu and Wang [18–22], Peralta and Laird [23], Zhang and Wang [24–28] and Zhang et al. [29,30], and the PSB-GB mechanism was established and perfected.

On the other hand, when adding alloy elements, such as zinc or aluminium, to copper, the cross slip frequency is reduced and the tendency for planar slip is increased. This planar slip behaviour is commonly correlated with the decrease in stacking fault energy (SFE). This gives rise to an interesting question as to how SFE affects the slip deformation and fatigue damage behaviour of those alloy materials. Some investigations found that there are no ladder-like PSBs after cyclic deformation for those Cu-based alloys, and their fatigue dislocation patterns are related to SFE [6]. Other investigations revealed that there is no clear saturation behaviour during the cyclic deformation of Cu-alloy single crystals [8,31]. However, Lukas et al. [32,33] and Wang [34] assumed that there are two plateaus in the CSSCs of Cu–22 wt% Zn and Cu–30 wt% Zn single crystals, when their CSSCs are established, based on different definitions of saturation stresses. Wang et al. [35] investigated the cyclic deformation behaviour of Cu–30 wt% Zn single crystals and found that the cyclic hardening behaviour strongly depends on the applied strain amplitude. To date, there is little information on strain-controlled cyclic plasticity in polycrystalline materials deformed by planar slip. An interesting question that emerged, however, from these investigations is whether or not there is true cyclic saturation prior to fatigue failure of α-brass. Another important question is whether there is an intrinsic difference in the fatigue cracking mechanisms along GBs and TBs due to the decrease in the SFE of α-brass. The main subject of the current study is to further identify the differences in cyclic deformation response and fatigue cracking mechanisms between pure copper and α-brass.

2. Experimental procedure

The materials used in this investigation are Cu (with an SFE of 40–78 mJ/m^2), Cu–10 wt% Zn (35 mJ/m^2) and Cu–32 wt% Zn (11–14 mJ/m^2) alloys [9,36,37]. Each material was supplied as a cold-rolled plate with a thickness of 4 mm. The fatigue specimens were spark machined from as-received plates, and the gauge dimension was $16 \times 5 \times 4$ mm. Before fatigue testing, all specimens were annealed at 800°C for 2 h in an Ar atmosphere. Then, the specimens were polished to produce a mirror-like surface for microscopic observation (the specimens of Cu, Cu–10 wt% Zn were electro-polished and those of Cu–32 wt% Zn were mechanically polished). The microstructures were investigated by scanning electron microscopy (SEM) and optical microscopy (OM). The average grain sizes

Table 1. Number of TBs in Cu, Cu–10 wt% Zn and Cu–32 wt% Zn alloys evaluated using different methods.

	$N_{TB}/(N_{TB}+N_{GB})$	N_{TB}/G	G_{TB}/G
Cu	57.5%	2.91	77.0%
Cu–10% Zn	54.8%	2.46	78.4%
Cu–32% Zn	51.9%	2.18	71.4%

N_{TB}: number of twin boundaries.
N_{GB}: number of grain boundaries.
G: number of grains.
G_{TB}: number of grains containing twins.

of Cu, Cu–10 wt% Zn and Cu–32 wt% Zn, which were measured by the line interception method, equalled 300–630, 210–355 and 195–315 μm, respectively. To evaluate the quantity of TBs, a large number of grains were explored in the three materials. The fraction of TBs within the population of TBs and GBs, the average quantity of TBs per grain and the percentage of grains containing TBs are listed in Table 1. Symmetrical pull–push cyclic deformation tests were performed at room temperature on a Shimadzu fatigue testing machine under constant plastic strain control mode. A triangular waveform with a frequency of 0.5 Hz was used as the control signal. The hysteresis loops were recorded continuously by computer. During the fatigue tests, the Cu specimens were cyclically deformed to the saturation stage and Cu–10 wt% Zn and Cu–32 wt% Zn specimens were cyclically deformed to a similar number of cycles at the same strain amplitude. At high plastic strain amplitudes ($\varepsilon_{pl} \geq 5 \times 10^{-4}$), the specimens were cyclically deformed to 5000 cycles or damaged before 5000 cycles. For $\varepsilon_{pl} = 2 \times 10^{-4}$ and 1×10^{-4}, the specimens were cyclically deformed to 10 000 and 15 000 cycles, respectively. After fatigue tests, the specimen surfaces were observed with a LEO Supra 35 field emission SEM.

3. Results and discussion

3.1. *Cyclic hardening*

The cyclic hardening curves of Cu, Cu–10 wt% Zn and Cu–32 wt% Zn alloys annealed at 800°C are shown in Figure 1. These curves were obtained by plotting the axial stress amplitude versus the number of cycles (N) on a semi-logarithmic scale. Several features can be observed from Figure 1a. Firstly, an obvious saturation stage can be seen after a certain amount of cyclic deformation of annealed pure copper. With the decrease in the plastic strain amplitude, the number of cycles to saturation increases while the saturation stress decreases. Secondly, in Figure 1b and c, the cyclic hardening behaviours of Cu–10 wt% Zn and Cu–32 wt% Zn strongly depend on the applied strain amplitude (ε_{pl}). When $\varepsilon_{pl} < 2 \times 10^{-3}$, the cyclic axial stress increases monotonously from the beginning of cycling and no clear saturation was detected for all the specimens tested within this strain range. However, when $\varepsilon_{pl} = 4 \times 10^{-3}$, the initial cyclic hardening and subsequent cyclic softening can be clearly seen, and then the saturation stage occurred in Cu–32 wt% Zn. The cyclic hardening behaviour of Cu–10 wt% Zn and Cu–32 wt% Zn strained at $\varepsilon_{pl} = 2 \times 10^{-3}$ seems to exhibit an intermediate behaviour.

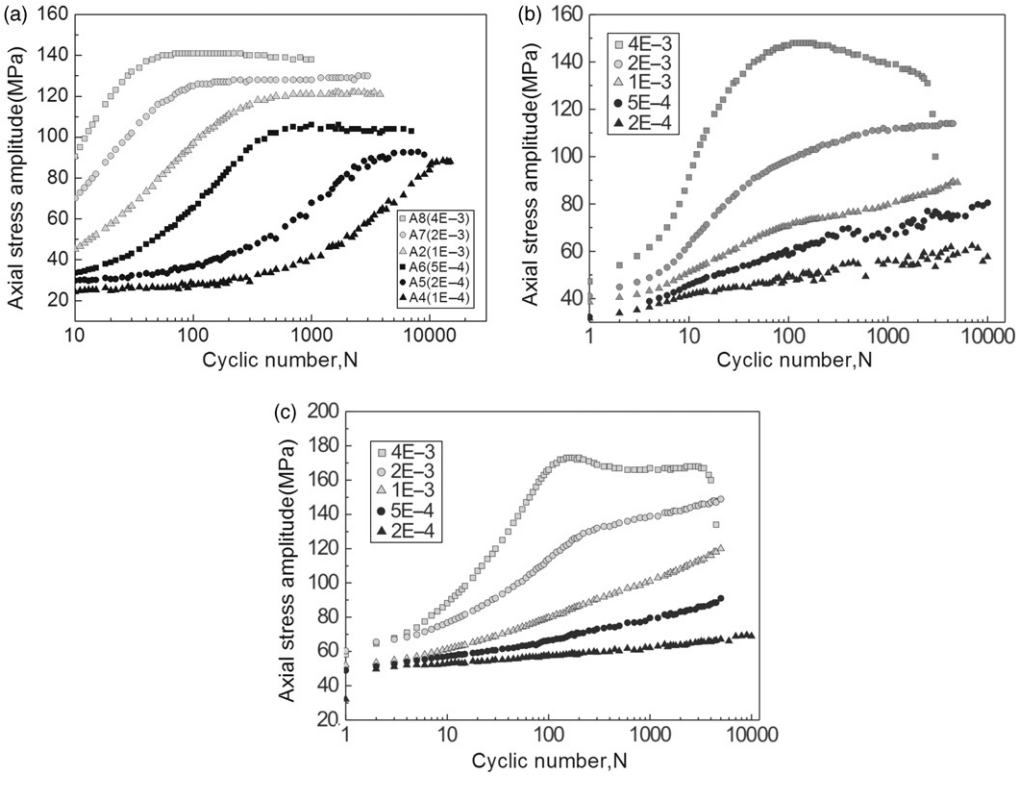

Figure 1. Cyclic hardening curves of polycrystalline (a) Cu, (b) Cu–10 wt% Zn, and (c) Cu–32 wt% Zn annealed at 800°C.

From the above experimental results, it can be seen that the cyclic hardening behaviour of pure copper differs from that of Cu–Zn alloys. Owing to its relatively high SFE, pure copper deforms under a typical wavy slip mode and its cyclic hardening behaviour is consistent with results obtained on Cu single crystals [1]. On the other hand, the low SFE of Cu–Zn alloys encourages planar-slip. The cyclic hardening behaviour of Cu–32 wt% Zn at low strain amplitude ($\varepsilon_{pl} \geq 2 \times 10^{-3}$) and Cu–10 wt% Zn is consistent with that previously found in Cu–Al crystals by Abel et al. [8] and Hong and Laird [31], whereas the cyclic hardening behaviour of Cu–32 wt% Zn alloy at high strain amplitude ($\varepsilon_{pl} = 4 \times 10^{-3}$) differs strongly from that of Cu–Al [8,31]. For $\varepsilon_{pl} = 4 \times 10^{-3}$, a saturation stage was observed after the cyclic softening stage without a second hardening stage.

3.2. *Cyclic stress–strain curves*

The cyclic stress–strain curves (CSSC) of pure Cu, Cu–10 wt% Zn and Cu–32 wt% Zn alloys are shown in Figure 2. The curves were obtained by plotting the axial saturation stress versus the plastic strain amplitude on a log–log scale. All the axial saturation stresses correspond to the cyclic stress amplitude at 2500 cycles because there is no clear cyclic

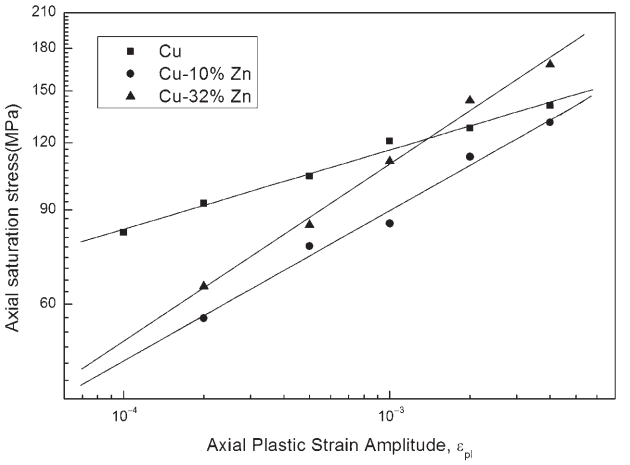

Figure 2. Cyclic stress–strain curves of polycrystalline Cu, Cu–10 wt% Zn and Cu–32 wt% Zn alloys annealed at 800°C.

saturation in Cu–Zn alloys. From Figure 2, it can be seen that these CSSCs can be approximated by straight lines, indicating that the saturation stress amplitude is a function of the plastic strain amplitude with a power law dependence, i.e.

$$\sigma_a = \sigma_f' \left(\frac{\varepsilon_{pl}}{\varepsilon_f'} \right)^{n'} . \tag{1}$$

where σ_f' is the fatigue strength coefficient, ε_f' is the fatigue ductility coefficient and n' is the cyclic strain hardening exponent [6]. The exponents calculated from Figure 2 for Cu, Cu–10 wt% Zn and Cu–32 wt% Zn amount to $n_1' = 0.15$, $n_2' = 0.28$ and $n_3' = 0.33$, respectively, indicating that the cyclic strain hardening exponent increases with decreasing the SFE.

3.3. *Surface deformation morphology*

After cyclic deformation, the surface deformation morphologies of pure Cu, Cu–10 wt% Zn and Cu–32 wt% Zn alloys were carefully observed by SEM to reveal the different slip modes and evolution of fatigue damage at different strain amplitudes. The surface slip traces of polycrystalline Cu deformed at low and high plastic strain amplitudes have similar features, and the morphology at $\varepsilon_{pl} = 1 \times 10^{-3}$ (5000 cycles) is shown in Figure 3. Many slip bands (SBs) were activated along different directions in both matrix and twin, but, due to crystal coherency at TBs, the SBs on both sides of TBs always exhibit a one-to-one relationship and they exhibit the same direction. These SBs always terminated at the GBs or TBs. Another feature of interest is that the intense and weak SBs appear alternatively, thus revealing a conspicuous plastic deformation localization, even in one grain or twin. This is consistent with the previous results in polycrystalline pure copper observed by Llanes and Laird [38].

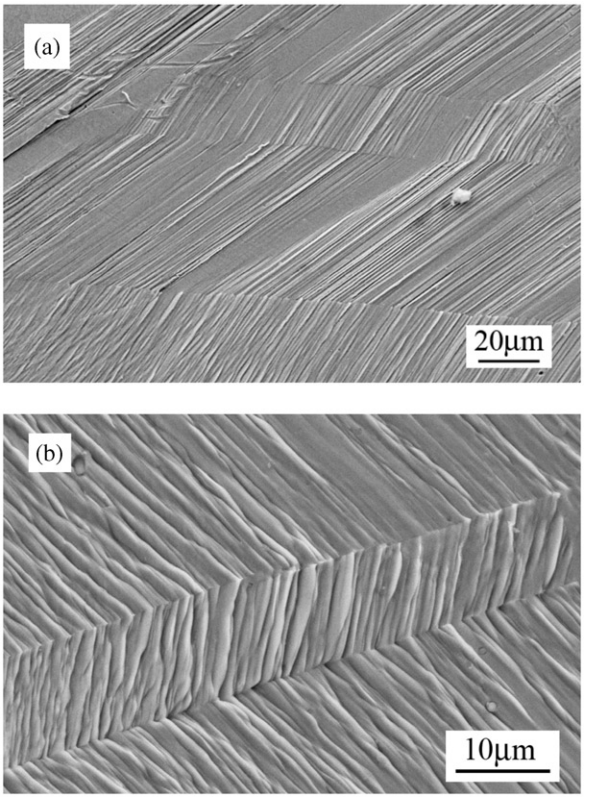

Figure 3. Surface slip morphologies near the TBs in fatigued polycrystalline Cu with strain amplitude (ε_{pl}): $\varepsilon_{pl} = 1 \times 10^{-3}$, $N = 5000$ cycles.

The surface slip traces of polycrystalline Cu–10 wt% Zn fatigued at different axial plastic strain amplitudes are shown in Figure 4. The specimens fatigued at low and high axial plastic strain amplitudes also show similar features. The SBs have similar directional relationship in both the matrix and the twin, but the SBs of Cu–10 wt% Zn are more homogeneous than those of pure copper, leading to weak plastic deformation localization in Cu–10 wt% Zn. Another feature is that many secondary SBs were observed near TBs, as shown in Figure 4c and d. Sometimes, the secondary SBs intersect with TB, such as in Figure 4c and sometimes the secondary SBs are parallel with TB, such as in Figure 4d. In the early studies of TB cracking behaviour, TBs with obvious parallel SBs easily nucleated fatigue cracks [39]. However, it has not been reported whether fatigue cracks could nucleate along TBs without obvious parallel slip bands. This question will be answered in following section.

The surface slip traces of polycrystalline Cu–32 wt% Zn cyclically deformed at different axial plastic strain amplitudes are shown in Figure 5. The directions of the SBs exhibit a one-to-one correspondence between the matrix and the twin, but the SBs of Cu–32 wt% Zn become more homogeneous than those of pure Cu and Cu–10 wt% Zn. The differences in surface slip traces between Cu and Cu–Zn alloys can be attributed to the different slip mode due to the variation of SFE [6].

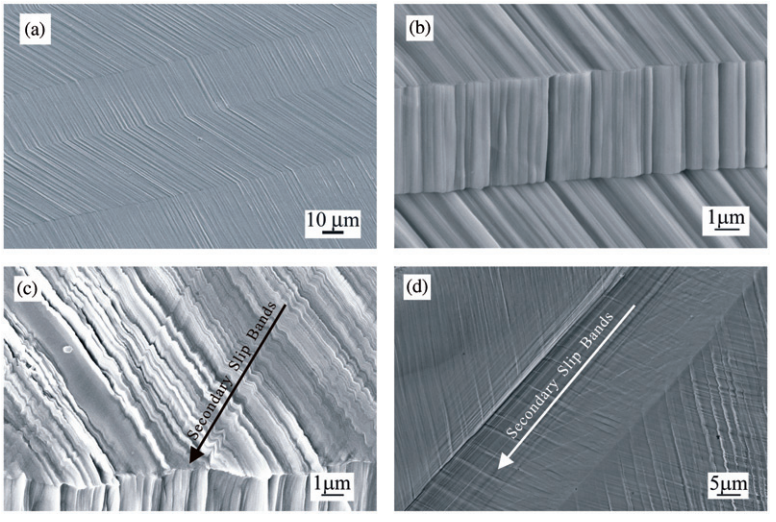

Figure 4. Surface slip morphologies near the twin boundaries in fatigued polycrystalline Cu–10 wt% Zn with different strain amplitudes (ε_{pl}): (a, b) $\varepsilon_{pl} = 1 \times 10^{-3}$, $N = 5000$ cycles (without secondary slip bands), (c) $\varepsilon_{pl} = 2 \times 10^{-3}$, $N = 5000$ cycles (with cross secondary slip bands), and (d) $\varepsilon_{pl} = 1 \times 10^{-3}$, $N = 5000$ cycles (with parallel secondary slip bands).

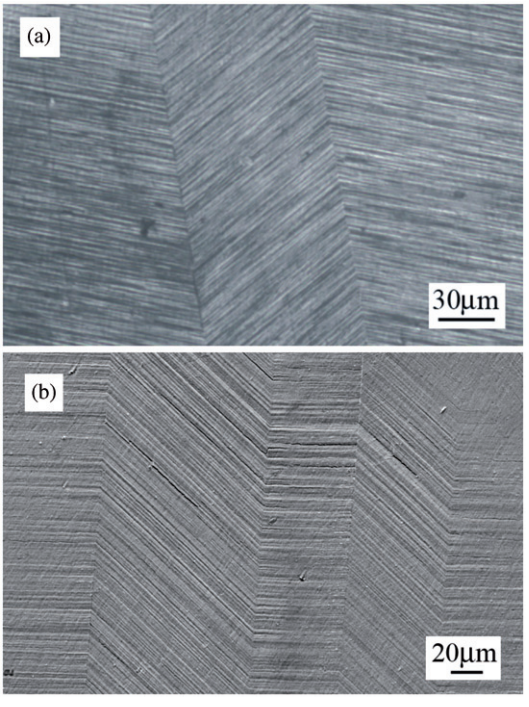

Figure 5. Surface slip morphologies near the TBs in fatigued polycrystalline Cu–32 wt% Zn alloy with different strain amplitudes (ε_{pl}): (a) $\varepsilon_{pl} = 1 \times 10^{-3}$, $N = 5000$ cycles and (b) $\varepsilon_{pl} = 4 \times 10^{-3}$, $N = 4300$ cycles.

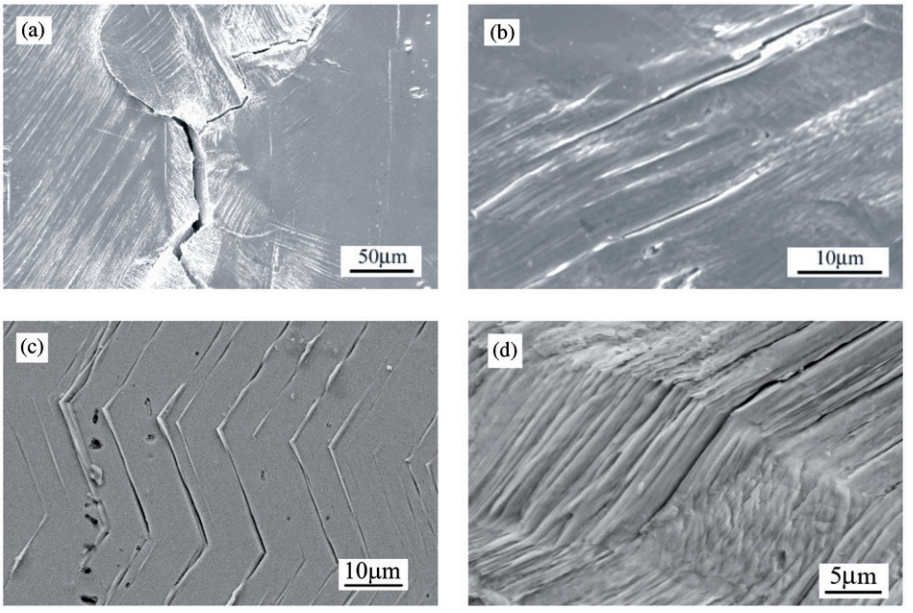

Figure 6. Fatigue cracking along (a) large angle boundaries ($\varepsilon_{pl} = 1 \times 10^{-3}$, $N = 15\,000$ cycles) and (b–d) persistent slip bands in fatigued polycrystalline Cu (b, c: $\varepsilon_{pl} = 1 \times 10^{-3}$, $N = 18\,000$ cycles; d: $\varepsilon_{pl} = 4 \times 10^{-3}$, $N = 1000$ cycles).

3.4. *Surface fatigue cracking*

The fatigue cracks on the surfaces of Cu, Cu–10 wt% Zn and Cu–32 wt% Zn were observed after cyclic deformation at different axial plastic strain amplitudes, as shown in Figures 6, 7 and 8, respectively. Based on numerous observations, it is found that the fatigue cracks nucleated frequently along GBs, as shown in Figures 6a, 7a and 8a. Sometimes, the fatigue cracks nucleate and propagate along SBs, as shown in Figures 6b–d, 7b and 8b. The phenomenon is in agreement with results in copper bicrystals [40] and in polycrystalline pure copper [41–43]. During the propagation of fatigue cracks, the GB crack sometimes propagated to a site where the preferential cracking occurred along SBs, so that the GB crack would change its path and became a SB crack. In the same way, the SB crack can become a GB crack. Via this mechanism, fatigue cracks can propagate along the intergranular and transgranular path alternately. When GB crack hits a triple junction of GB, it can simultaneously propagate along multiple GBs.

In addition to the common GBs in polycrystalline copper and Cu–Zn alloys, there are many TBs after annealing at 800°C. Fatigue cracking was frequently observed along GBs but none along the TBs in pure copper. The fatigue cracks can nucleate along SBs and propagate across TB, as shown in Figures 6c, d. There are also several SB cracks propagating across TB in Cu–Zn alloys, as in pure copper, but the difference is that fatigue cracks can frequently nucleate and propagate along the annealing TBs in Cu–Zn alloys, as shown in Figures 7c, d and 8c, d. It should be pointed out that the fatigue cracking behaviour near TB in Cu–10 wt% Zn alloy (with medium content of Zinc) exhibited the

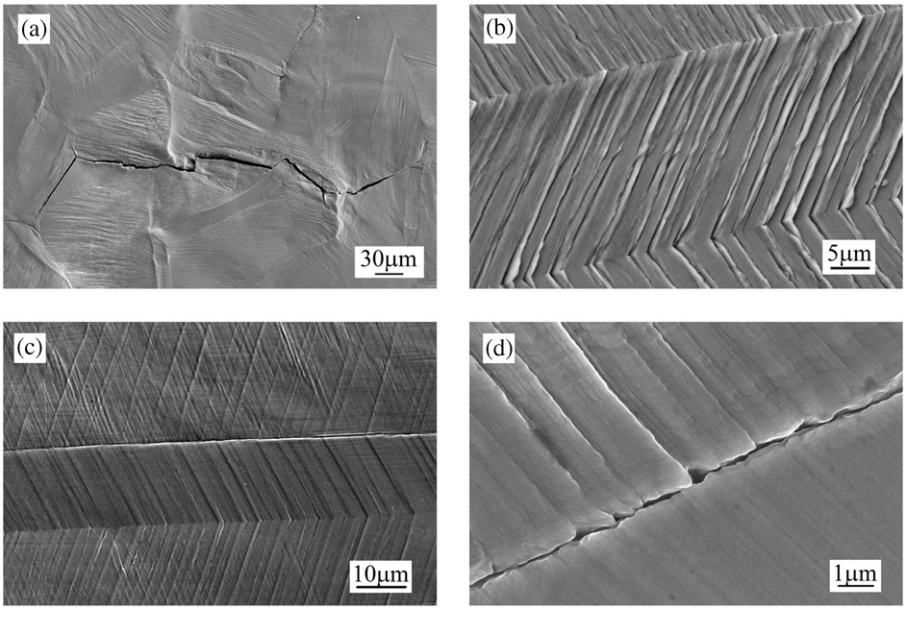

Figure 7. Fatigue cracking along (a) large-angle GBs (b) PSBs and (c, d) TBs in fatigued polycrystalline Cu–10 wt% Zn alloy ($\varepsilon_{pl} = 4 \times 10^{-3}$, $N = 3236$ cycles).

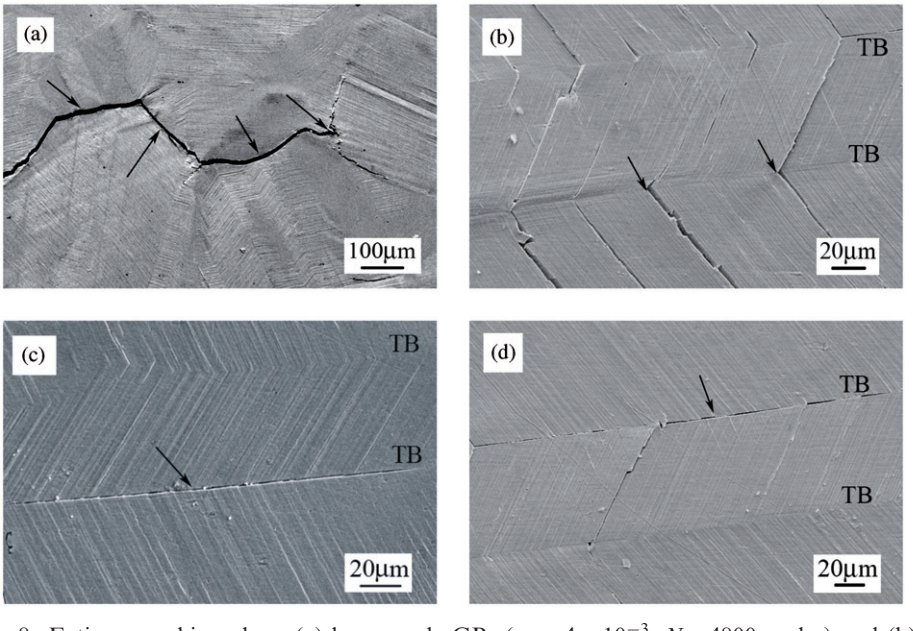

Figure 8. Fatigue cracking along (a) large-angle GBs ($\varepsilon_{pl} = 4 \times 10^{-3}$, $N = 4800$ cycles) and (b) SBs ($\varepsilon_{pl} = 4 \times 10^{-3}$, $N = 4000$ cycles), and (c, d) TBs ($\varepsilon_{pl} = 4 \times 10^{-3}$, $N = 4000$ cycles) in fatigued polycrystalline Cu–32 wt% Zn alloy.

intermediate character between Cu and Cu–32 wt% Zn. Fatigue cracking along TB could be observed in Cu–10 wt% Zn alloy, but was less frequent than in Cu–32 wt% Zn alloy; fatigue cracking nucleated along SBs near TB was observed more frequently.

In addition, several TB cracks were observed by SEM in Cu–10 wt% Zn, as shown in Figure 7c and d. The phenomenon of fatigue cracks nucleating along TBs with parallel SBs has been discussed previously. However, it was observed that fatigue cracks nucleate along TBs without any evidence of parallel SBs being formed, raising the question as to whether different fatigue cracking mechanisms exist between the TBs with or without parallel SBs. Slip traces near TB cracks were observed in Cu–32 wt% Zn. More TB cracks were observed than in Cu and Cu–10 wt% Zn alloy, as shown in Figure 8c and d. TB cracks without parallel SBs were frequently observed, while TB cracks with parallel SBs were difficult to find.

These properties suggest that the fatigue cracking mechanisms between TB cracks with and without parallel SBs are different. These differences will be discussed in terms of the SFE.

3.5. *TB cracking mechanisms*

There have been several classical contributions to the understanding of the TB crack mechanism. Boettner et al. [39] discussed the relationship between the slip plane and TB, and considered that the formation of TB cracks during fatigue requires the operation of slip planes parallel to the TB. Using a finite element program, Wang et al. [44] calculated the stress distribution near TBs have three different orientations with stress axis, and Neumann et al. [45] calculated the misfit stresses at GBs using a simple method. Following the ideas of Neumann [45], Heinz and Neumann [46] developed an analytical model to calculate surface tractions near TBs caused by the elastic anisotropy of twins. Subsequently, Blochwitz and Tirschler [47] explained the TB cracking mechanism in terms of additional stress components stress superimposed on the applied stress components arising from displacement compatibility requirements at TBs. All these studies paid particular attention to the relationship between the slip bands and TBs, which exhibits no essential difference between copper and Cu–Zn alloys. Nevertheless, it has been widely observed that the fatigue cracking mechanisms are quite different between GBs and TBs in various polycrystalline materials [38,47–49] and these differences have not been properly explained so far. In particular, the models cannot explain why, in Cu–Zn alloys, fatigue cracking occurs along TBs with parallel SBs.

Based on our observations, the TB cracking mechanism can be classified as two types. Firstly, type A TB cracks, where fatigue cracking nucleates along TBs with parallel SBs (Figure 9), as discussed in early studies [39]. It was assumed that the TB cracks only nucleate under specific situations, which require SBs to be parallel to the TBs; as a result, type A TB cracks are rarely observed.

Secondly, micro-cracking can nucleate in a number of situations, as shown in Figure 10. The secondary SBs (weak parallel SBs and intersecting SBs) could strike the primary SBs, forming very fine cracks, both in and close to TBs, as indicated by the arrow in Figure 10a and b. Occasionally, there are no secondary SBs near the TB, but micro-cracks were still observed, as shown in Figure 10c and d, which can be explained if TBs could block dislocation motion, as with conventional GBs [50–52]. Based on

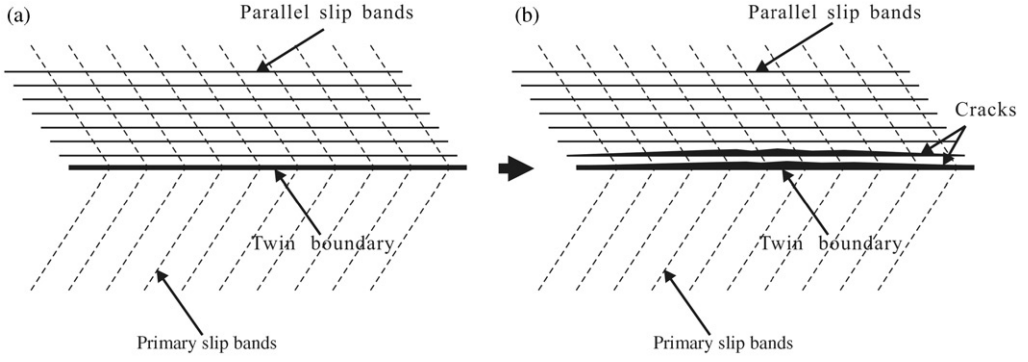

Figure 9. Scheme for type A TB cracking behaviour: cracks nucleated along TB due to parallel SBs.

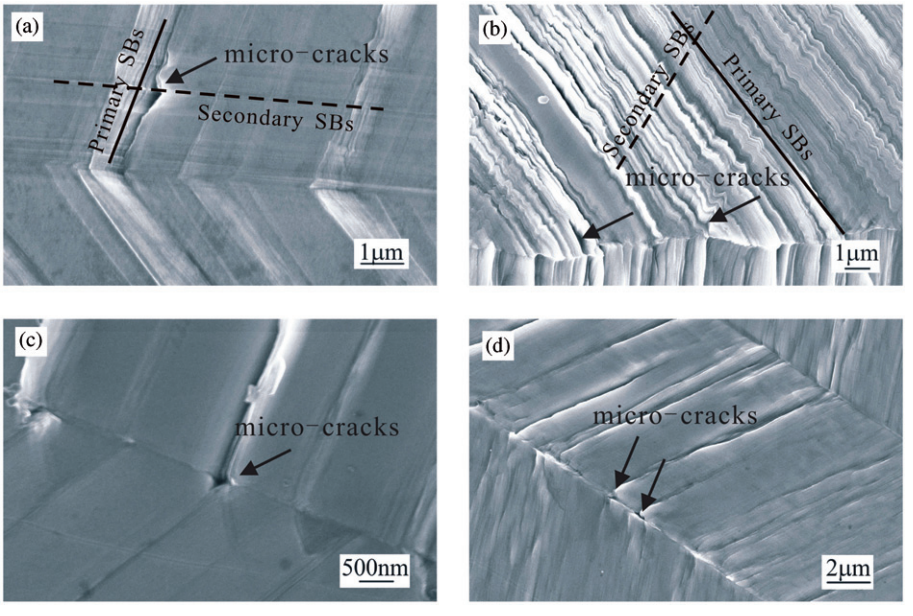

Figure 10. Fatigue micro-cracks nucleated near TBs in fatigued polycrystalline Cu–10 wt% Zn alloy ($\varepsilon_{pl} = 4 \times 10^{-3}$, $N = 3236$ cycles).

these observations, a different TB cracking mechanism was assumed (Figure 11). These micro-cracks connect with each other, leading to the final TB cracks during cyclic deformation. This type of TB cracking is designated as type B TB cracks; the processes of nucleation and connection of these micro-cracks are illustrated in Figure 11. These TB cracks are independent of the relationship between the direction of the applied stress and the TB. From our results, type B TB cracks should be readily observed, primarily, in Cu–Zn alloys with low SFE, as will be discussed below.

It is apparent that the slip morphologies are different between pure Cu and Cu–Zn alloys with high and low SFE, as shown in Figures 12a, d and 13a, e. Therefore, it is

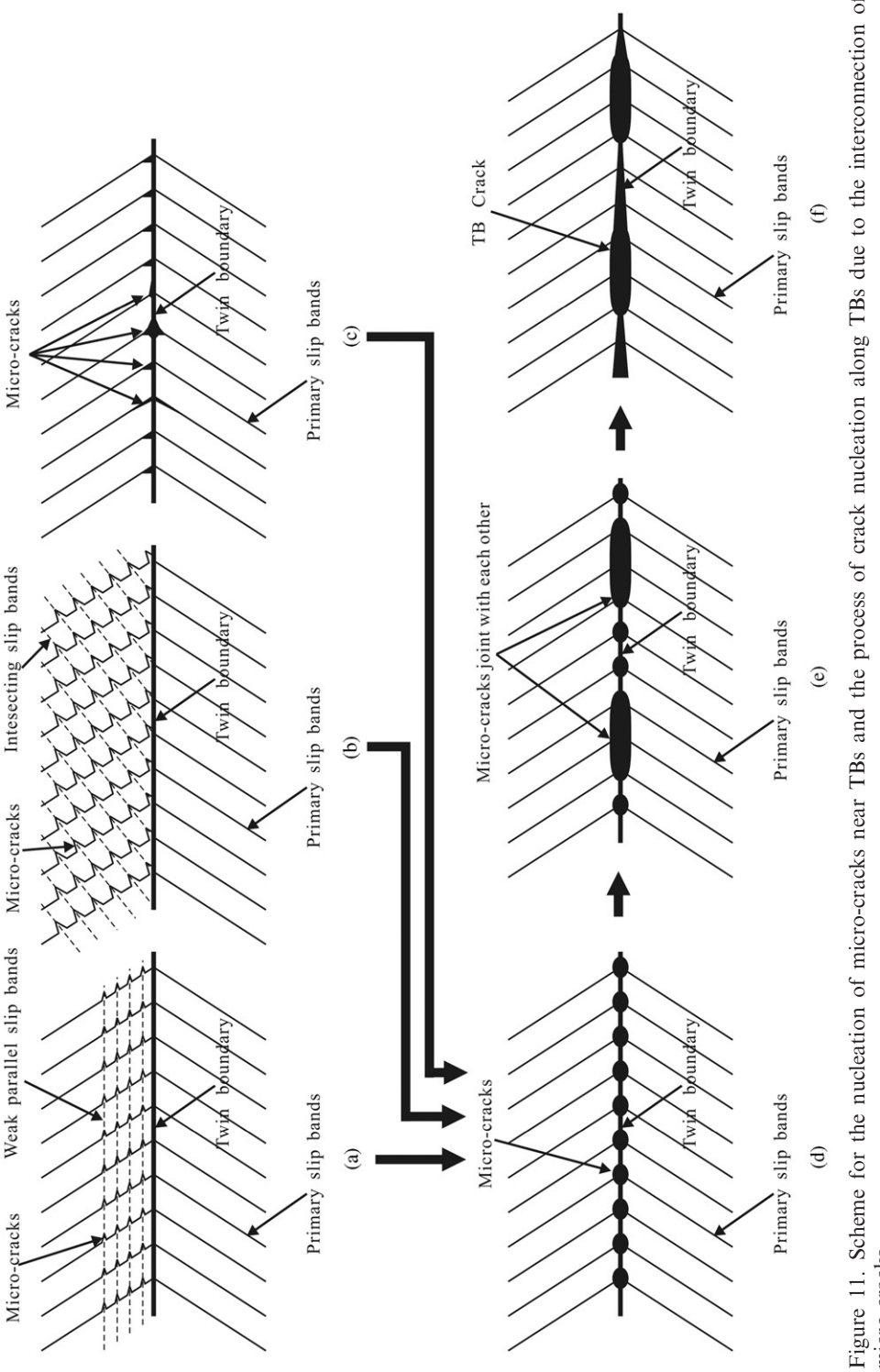

Figure 11. Scheme for the nucleation of micro-cracks near TBs and the process of crack nucleation along TBs due to the interconnection of micro-cracks.

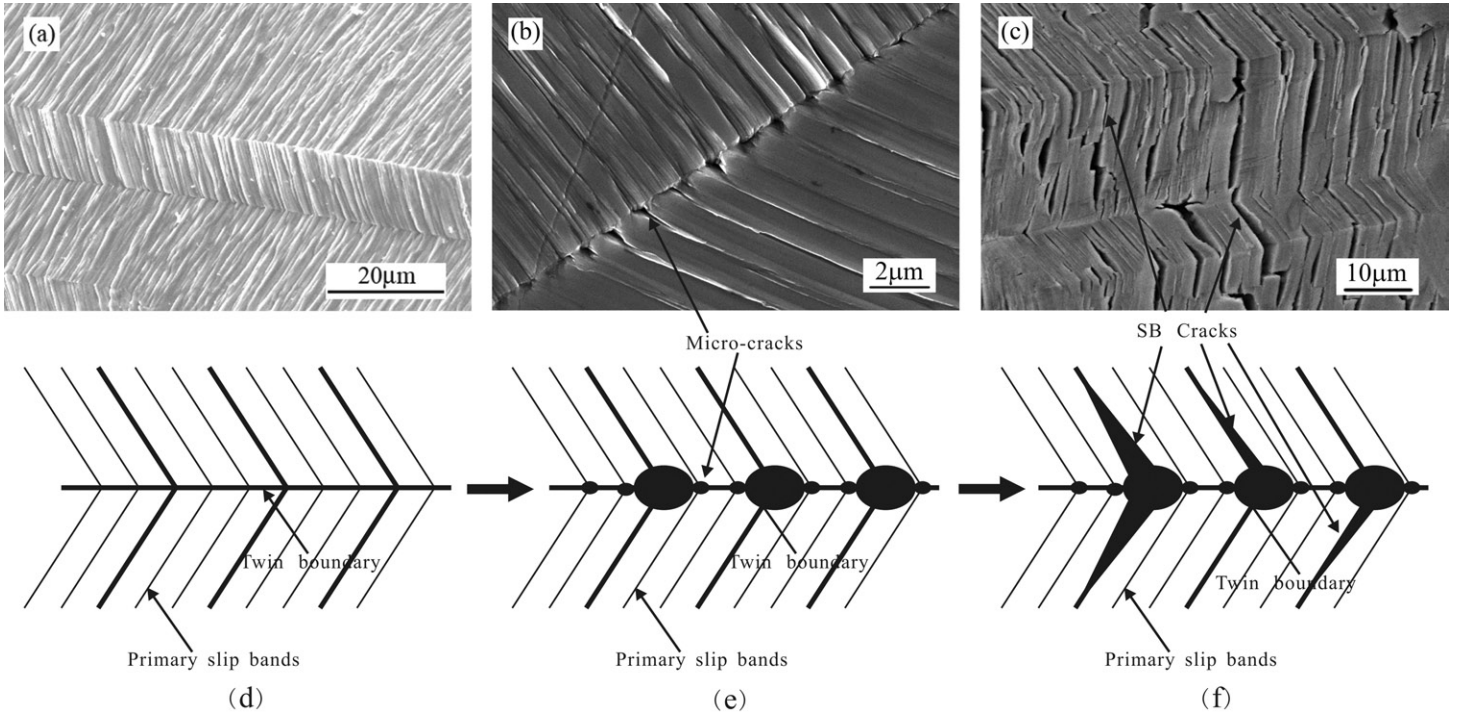

Figure 12. Scheme for fatigue cracks nucleated along SBs in materials with a high SFE. (a) Cu, $\varepsilon_{pl} = 1 \times 10^{-3}$, $N = 10\,000$ cycles, (b) Cu–10 wt% Zn, $\varepsilon_{pl} = 4 \times 10^{-3}$, $N = 3236$ cycles, and (c) Cu, $\varepsilon_{pl} = 4 \times 10^{-3}$, $N = 1000$ cycles.

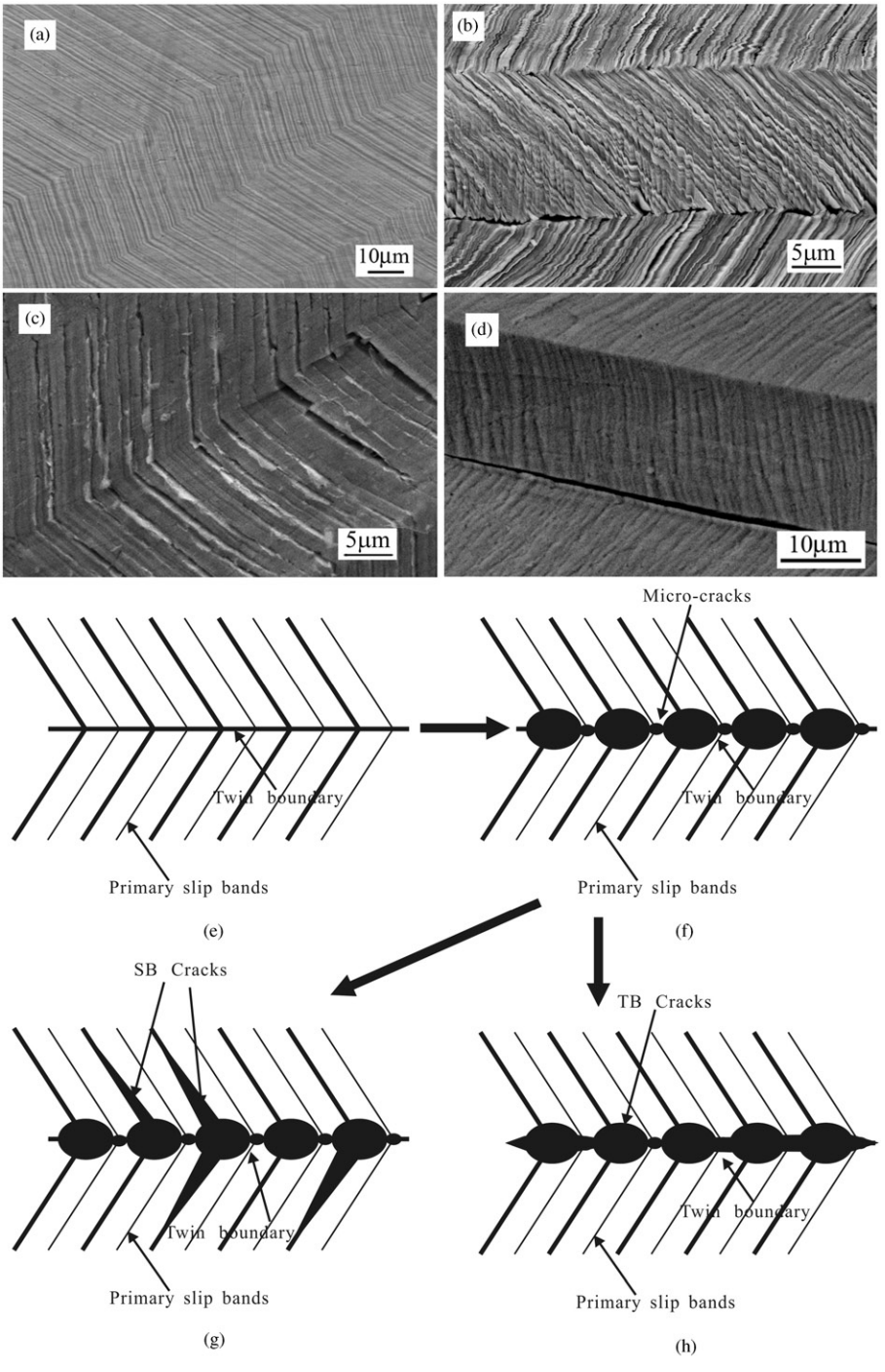

Figure 13. Scheme for fatigue cracks nucleated along SBs and TBs in materials with a low SFE. (a) Cu–32% Zn, $\varepsilon_{pl} = 1 \times 10^{-3}$, $N = 5000$ cycles, and (b–d) Cu–32 wt% Zn, $\varepsilon_{pl} = 4 \times 10^{-3}$, $N = 4000$ cycles.

possible that there are two different cracking modes near the TBs, as illustrated in Figures 12 and 13. Thus, it was found that the micro-cracks could nucleate near TBs during cyclic deformation. In pure Cu with a high SFE, the localization of SBs is more pronounced and there is a large space between micro-cracks with intense deformation, as shown in Figure 12b and e. Therefore, these micro-cracks are difficult to interconnect and will propagate along slip bands, as shown in Figure 12c and f. In Cu–Zn alloy with a low SFE, the SBs are more homogeneous than in pure Cu with a high SFE, and the micro-cracks with intense deformation are closer, as shown in Figure 13b and f. Therefore, fatigue cracks could nucleate along two different paths. One possibility is that the micro-cracks could propagate along SBs, resulting in SB cracking, which is similar to the PSB cracking mechanism in pure Cu with a high SFE [4,13,14], as shown in Figure 13c and g. Another possibility is that the micro-cracks accompanying intense deformation interconnect more easily, forming cracks along the TB, as shown in Figure 13d and h. For Cu–32 wt% Zn alloy, it was found that type B TB cracking becomes much easier because the slip morphology is more homogeneous, which in turn can be attributed to the decrease in SFE. In other words, our observations provide new evidence that the TB cracking displays clear differences in pure Cu and Cu–Zn alloys, which should assist the design of alloys with high fatigue resistance.

4. Conclusions

(1) The cyclic hardening behaviour of pure Cu differs from that of Cu–Zn alloys. In pure Cu, an obvious saturation stage can be seen after a certain degree of cyclic deformation, whereas there is no obvious saturation stage in Cu–32 wt% Zn alloy at low strain amplitudes ($\varepsilon_{pl} \leq 2 \times 10^{-3}$) or in Cu–10 wt% Zn. Cyclic softening takes place before cyclic saturation in Cu–32 wt% Zn alloy at high strain amplitude ($\varepsilon_{pl} = 4 \times 10^{-3}$).

(2) The cyclic stress–strain curve (CSSC) plotted on a log-log scale can be approximated by a straight line whose slope increases with decreasing SFE in Cu–Zn alloys.

(3) The surface slip morphologies are different between Cu, Cu–10 wt% Zn and Cu–32 wt% Zn. The surface slip traces for pure Cu with a high SFE exhibit an apparent wavy behaviour with intense SBs and severe strain localization. With decreasing SFE in Cu–Zn alloys, the surface slip trace becomes more homogenous with less strain localization.

(4) The fatigue cracks can nucleate along GBs or SBs in both pure Cu and Cu–Zn alloys. In addition, as the SFE decreases, fatigue cracks readily nucleate along annealing TBs. The intrinsic difference in the TB cracking behaviour between pure Cu and Cu–Zn alloys can be attributed to the degree of plastic strain concentration, as revealed by surface slip traces.

Acknowledgements

The authors thank W. Gao, H. H. Su, J. L. Wen, and G. Yao for sample preparation, mechanical tests and SEM observations. This work was financially supported by the "Hundred of Talents

Project'' by the Chinese Academy of Sciences and the National Natural Science Funding of China (NSFC) under grant Nos. 50571104 and 50625103.

References

[1] H. Mughrabi, Mater. Sci. Eng. 33 (1978) p.207.
[2] J.C. Swearengen and R. Taggart, Acta Metall. 19 (1971) p.543.
[3] D. Kuhlmann-Wilsdorf and C. Laird, Mater. Sci. Eng. 27 (1977) p.137.
[4] A.T. Winter, O.R. Pedersen and K.V. Rasmussen, Acta Metall. 29 (1981) p.735.
[5] C. Laird, P. Charsley and H. Mughrabi, Mater. Sci. Eng. 81 (1986) p.433.
[6] P. Lukas and M. Klesnil, Mater. Sci. Eng. 11 (1973) p.345.
[7] J.M. Finney and C. Laird, Philos. Mag. A 31 (1975) p.339.
[8] A. Abel, M. Wilhelm and V. Gerold, Mater. Sci. Eng. 37 (1979) p.187.
[9] Z.R. Wang, Philos. Mag. 84 (2004) p.351.
[10] A.S. Cheng and C. Laird, Mater. Sci. Eng. 51 (1981) p.111.
[11] Z.F. Zhang and Z.G. Wang, Philos. Mag. A 81 (2001) p.399.
[12] A.T. Winter, Philos. Mag. A 30 (1974) p.719.
[13] U. Essmann, U. Gosele and H. Mughrabi, Philos. Mag. A 44 (1981) p.405.
[14] K. Differt, U. Essmann and H. Mughrabi, Philos. Mag. A 54 (1986) p.237.
[15] J. Waltersdorf and H. Vehoff, Scripta Metall. 23 (1989) p.513.
[16] P. Gopalan and H. Margolin, Mater. Sci. Eng. A 142 (1991) p.11.
[17] Y.M. Hu, Z.G. Wang and G.Y. Li, Mater. Sci. Eng. A 208 (1996) p.260.
[18] Y.M. Hu and Z.G. Wang, Scripta Mater. 35 (1996) p.1019.
[19] Y.M. Hu and Z.G. Wang, Acta Mater. 45 (1997) p.2655.
[20] Y.M. Hu and Z.G. Wang, Mater. Sci. Eng. A 234/236 (1997) p.98.
[21] Y.M. Hu and Z.G. Wang, Int. J. Fatigue 20 (1998) p.463.
[22] Y.M. Hu, Z.G. Wang and S.X. Li, J. Mater. Sci. Lett. 17 (1998) p.1773.
[23] P. Peralta and C. Laird, Acta Mater. 45 (1997) p.3029.
[24] Z.F. Zhang and Z.G. Wang, Philos. Mag. Lett. 78 (1998) p.105.
[25] Z.F. Zhang and Z.G. Wang, Mater. Sci. Eng. A 255 (1998) p.148.
[26] Z.F. Zhang and Z.G. Wang, Acta Mater. 46 (1998) p.5063.
[27] Z.F. Zhang and Z.G. Wang, Philos. Mag. A 79 (1999) p.741.
[28] Z.F. Zhang and Z.G. Wang, Prog. Mater. Sci. 53 (2008) p.1025.
[29] Z.F. Zhang, Z.G. Wang and Y.M. Hu, Mater. Sci. Eng. A 269 (1999) p.136.
[30] Z.F. Zhang, Z.G. Wang and S.X. Li, Fatigue Fract., Eng. Mater. Struct. 21 (1998) p.1307.
[31] S.I. Hong and C. Laird, Mater. Sci. Eng. A 128 (1990) p.55.
[32] P. Lukas, L. Kunz, Z. Cochnar et al., Mater. Sci. Eng. A 145 (1991) p.L19.
[33] P. Lukas, L. Kunz and J. Krejci, Mater. Sci. Eng. A 158 (1992) p.177.
[34] Z. Wang, Mater. Sci. Eng. A 183 (1994) p.13.
[35] Z. Wang, B. Gong and Z.G. Wang, Acta Mater. 47 (1998) p.307.
[36] P.C.J. Gallagher, Metall. Trans. 1 (1970) p.2429.
[37] L.E. Murr, *Interfacial free energy*, in *Interfacial phenomena in metals and alloys*, L.E. Murr ed., Addison-Wesley, MA, 1975, pp. 145–148.
[38] L. Llanes and C. Laird, Mater. Sci. Eng. A 157 (1992) p.21.
[39] R.C. Boettner, A.J. McEvily and Y.C. Liu, Philos. Mag. 10 (1964) p.95.
[40] Z.F. Zhang and Z.G. Wang, Acta Mater. 51 (2003) p.347.
[41] J.C. Figueroa and C. Laird, Mater. Sci. Eng. 60 (1983) p.45.
[42] W. Liu, M. Bayerlein, H. Mughrabi et al., Acta Metall. Mater. 40 (1992) p.1763.
[43] H.L. Huang and N.J. Ho, Mater. Sci. Eng. A 293 (2000) p.7.
[44] Z. Wang and H. Margolin, Metall. Trans. A 16 (1985) p.873.

[45] P. Neumann and A. Tönnessen, *Crack initiation at grain boundaries in F.C.C. materials*, in *Strength of Metals and Alloys*, P.O. Kettunen, T.K. Lepisto and M.E. Lehtonen eds., Pergamon Press, Oxford, 1988, pp. 743–748.
[46] A. Heinz and P. Neumann, Acta Metall. Mater. 38 (1990) p.1933.
[47] C. Blochwitz and W. Tirschler, Cryst. Res. Technol. 40 (2005) p.32.
[48] C. Blochwitz, R. Richter, W. Tirschler et al., Mater. Sci. Eng. A 234 (1997) p.563.
[49] C. Blochwitz and W. Tirschler, Mater. Sci. Eng. A 339 (2003) p.318.
[50] J.W. Christian and S. Mahajan, Prog. Mater Sci. 39 (1995) p.1.
[51] S.D. Dahlgren, W.L. Nicholson, M.D. Merz et al., Thin Solid Films 40 (1977) p.345.
[52] L. Lu, Y.F. Shen, X.H. Chen et al., Science 304 (2004) p.422.